Scientific Reports

https://doi.org/10.1038/s41598-026-40709-x

Article in Press

Targeted activation of Nrf2 via sulforaphane-loaded exosomes attenuated azoospermic condition in the rat model

Received: 18 October 2025

Accepted: 16 February 2026

Published online: 18 February 2026

Cite this article as: Ahmadian S., Fajri M., Roelen B.A. *et al.* Targeted activation of Nrf2 via sulforaphane-loaded exosomes attenuated azoospermic condition in the rat model. *Sci Rep* (2026). https://doi.org/10.1038/s41598-026-40709-x

Shahin Ahmadian, Mehrsa Fajri, Bernard A.J. Roelen, Ali Abedelahi, Mehdi Talebi, Reza Rahbarghazi & Mahdi Mahdipour

Targeted Activation of Nrf2 via Sulforaphane-Loaded Exosomes attenuated Azoospermic condition in the Rat model

Shahin Ahmadian[1,2], Mehrsa Fajri[1], Bernard A.J. Roelen[3], Ali Abedelahi[2,4], Mehdi Talebi[2,5], Reza Rahbarghazi[2, 6], Mahdi Mahdipour[1,2,7*]

[1] Stem Cell Research Center, Tabriz University of Medical Sciences, Tabriz, Iran

[2] Department of Applied Cell Sciences, Faculty of Advanced Medical Sciences, Tabriz University of Medical Sciences, Tabriz, Iran

[3] Department Clinical Sciences, Faculty of Veterinary Medicine, Utrecht University, Utrecht, The Netherlands

[4] Department of Anatomical Sciences, Faculty of Medicine, Tabriz University of Medical Sciences, Tabriz, Iran

[5] Hematology and Oncology Research Center, Tabriz University of Medical Sciences, Tabriz, Iran

[6] Stem Cell and Regenerative Medicine Institute (SCARM), Tabriz University of Medical Sciences, Tabriz, Iran.

[7] Department of Reproductive Biology, Faculty of Advanced Medical Sciences, Tabriz University of Medical Sciences, Tabriz, 5166653431, Iran

*Address for correspondence: Dr. Mahdi Mahdipour (Ph.D.), Stem Cell Research Center, Tabriz University of Medical Sciences, and Department of Reproductive Biology, Faculty of Advanced Medical Sciences, Tabriz University of Medical Sciences, Daneshghah St. Tabriz, 5166615739, Iran; Telefax: +98-41-3336-3870; E-mail: mahdipourm@tbzmed.ac.ir; mahdi.mahdipour@gmail.com

Running title: **Spermatogenesis Recovery with Nrf2-activating exosomes**

Highlights

1. Human serum-derived exosomes were successfully engineered to encapsulate sulforaphane (SFN) using an ultrasonication-based method, achieving about 47% indirect loading efficiency.

2. Intratesticular delivery of SFN-loaded exosomes significantly restored sperm count, motility and morphology in busulfan-induced azoospermic rats.

3. Histopathological analyses showed improved germ cell recovery and reduced testicular fibrosis in the SFN-loaded exosome (SFN+EXO) group compared to monotherapies.

4. SFN+EXO treatment normalized expression of spermatogenic (*DAZL*, *VASA*), oxidative stress (*Nrf2*) and autophagy markers (*LC3*, *Beclin1*, *p62*).

5. Combination therapy outperformed SFN or exosomes alone, offering a promising approach for treating male infertility via modulation of Nrf2 and autophagic pathways.

Abstract

Background: Azoospermia, the complete absence of sperm in the ejaculate, presents a major barrier to male fertility. Oxidative stress and impaired cellular homeostasis are key contributors to germ cell loss, particularly in chemotherapy-induced azoospermia. Sulforaphane (SFN), a potent activator of the Nrf2 pathway, offers antioxidant benefits, but its systemic delivery is limited by bioavailability and potential reductive stress. This study aimed to evaluate the regenerative potential of SFN-loaded exosomes (SFN+EXO) in a rat model of azoospermia.

Methods: Human serum-derived exosomes were isolated, characterized and engineered to encapsulate SFN. Azoospermia was induced in Wistar rats via intratesticular busulfan injection. Animals were assigned to five groups: healthy control, azoospermic control, SFN, exosomes (EXO) and SFN+EXO. Spermatogenesis parameters, histopathology, testosterone levels, oxidative stress markers and gene expression of *Nrf2*, autophagy and germ cell markers were evaluated.

Results: SFN+EXO treatment significantly improved sperm count, motility, morphology and testis weight index compared to controls and monotherapy groups. Histological recovery of spermatogenic lineages was superior in SFN+EXO rats, accompanied by reduced fibrosis and normalized testicular architecture. Expression of DAZL and VASA was fully restored, while aberrant upregulation of *Nrf2* and autophagy genes (*LC3*, *Beclin1*, *p62*) in azoospermic testes was normalized only by SFN+EXO. Antioxidant enzyme activity (GPx, TAC) was significantly enhanced, suggesting redox balance recovery.

Conclusions: Local delivery of sulforaphane via exosomes effectively reverses chemotherapy-induced spermatogenic failure through modulation of oxidative stress and autophagy, promoting germ cell regeneration. This exosome-based platform offers a promising therapeutic avenue for male infertility.

Keywords: Azoospermia, Sulforaphane, Exosomes, Oxidative stress, Autophagy, Spermatogenesis

1. Background

Infertility is a significant global health challenge in reproductive medicine, with nearly 17.5% of people globally affected (1). Male infertility is responsible for approximately 50% of these cases. Among the various causes of infertility, azoospermia, characterized by the complete or almost complete absence of spermatozoa in the ejaculate, is one of the most severe and challenging conditions to treat. Current therapeutic approaches are often inadequate in restoring endogenous spermatogenesis in azoospermia, leaving very few options for achieving biological paternity in many patients (2-5).

Azoospermia can arise from diverse etiologies including genetic abnormalities, obstructive causes and primary testicular failure (5). Oxidative stress functions as a critical downstream mediator of germ cell damage in specific forms of non-obstructive azoospermia, particularly those induced by chemotherapeutic agents such as busulfan (5). Oxidative stress occurs when the balance between the production of reactive oxygen species (ROS) and cellular antioxidant defenses is disrupted, which will cause extensive molecular damage (6, 7). Spermatogenesis which is the process of producing sperm in the testes, is a highly precise process that can be disrupted by multiple factors, including genetic defects, environmental toxins and oxidative stress (7). In the testicular environment, excessive ROS not only damages cell membranes, proteins and DNA, but also compromises the integrity of the seminiferous tubules, which is a natural niche for germ cell development (8). This oxidative damage plays a key role in the events that lead to impaired spermatogenesis and ultimately male infertility (9, 10).

In recent years, nuclear factor erythroid-related factor 2 (Nrf2) has emerged as a key regulator of the cellular antioxidant response (11). Nrf2 coordinates the expression of a wide range of genes that are critical for ROS detoxification and reduction of oxidative damage (12). Given its pivotal role in maintaining redox homeostasis, Nrf2 activation is an attractive therapeutic target for conditions characterized by oxidative stress (13) and can provide an environment for cellular repair and regeneration (14). A well-established and potent natural activator of the Nrf2 pathway is sulforaphane, a bioactive isothiocyanate found in cruciferous vegetables (15, 16). Sulforaphane can pharmacologically activate Nrf2 mainly through covalent modification of specific cysteine residues on Kelch Like ECH Associated Protein 1 (Keap1), which disrupts Keap1-mediated ubiquitination and proteasomal degradation of Nrf2. This, leads to Nrf2 stabilization, nuclear translocation, and transcriptional activation of antioxidant response genes (15, 16). The ability of this compound to upregulate cellular defense mechanisms has been demonstrated, which offers promising insights into its potential application in overcoming oxidative damage (15).

Despite its promise, the clinical use of sulforaphane is limited by its poor stability and low bioavailability in free form (17, 18). For therapeutic application in the testicular microenvironment, an optimal delivery system should protect sulforaphane from rapid degradation. Exosomes, as endogenous nanoscale vesicles, fulfill these criteria by providing a biocompatible and protective carrier capable of enhancing payload stability and tissue retention. In recent years, the use of exosome-mediated drug delivery has attracted much attention. Exosomes, as natural nanocarriers (30 to 150 nm), offer several advantages, including enhanced stability, low immunogenicity and the potential to cross biological barriers (5, 19). This novel drug delivery system allows for the encapsulation of sulforaphane and release directly into the testicular microenvironment, resulting in enhanced therapeutic potential (17, 20, 21).

The current study hypothesized that activating the Nrf2 signaling pathway through localized delivery of exosome encapsulated sulforaphane may improve spermatogenesis in a busulfan-induced non-obstructive azoospermia rat model (**Figure 1**). Taking advantage of the natural benefits of exosomes, this study aimed to increase the concentration and local efficacy of sulforaphane, in order to ultimately improve testicular function. The findings may not only increase our understanding of the molecular interplay between Nrf2 activation and testicular repair, but could also pave the way for regenerative medicine against oxidative stress-related disorders.

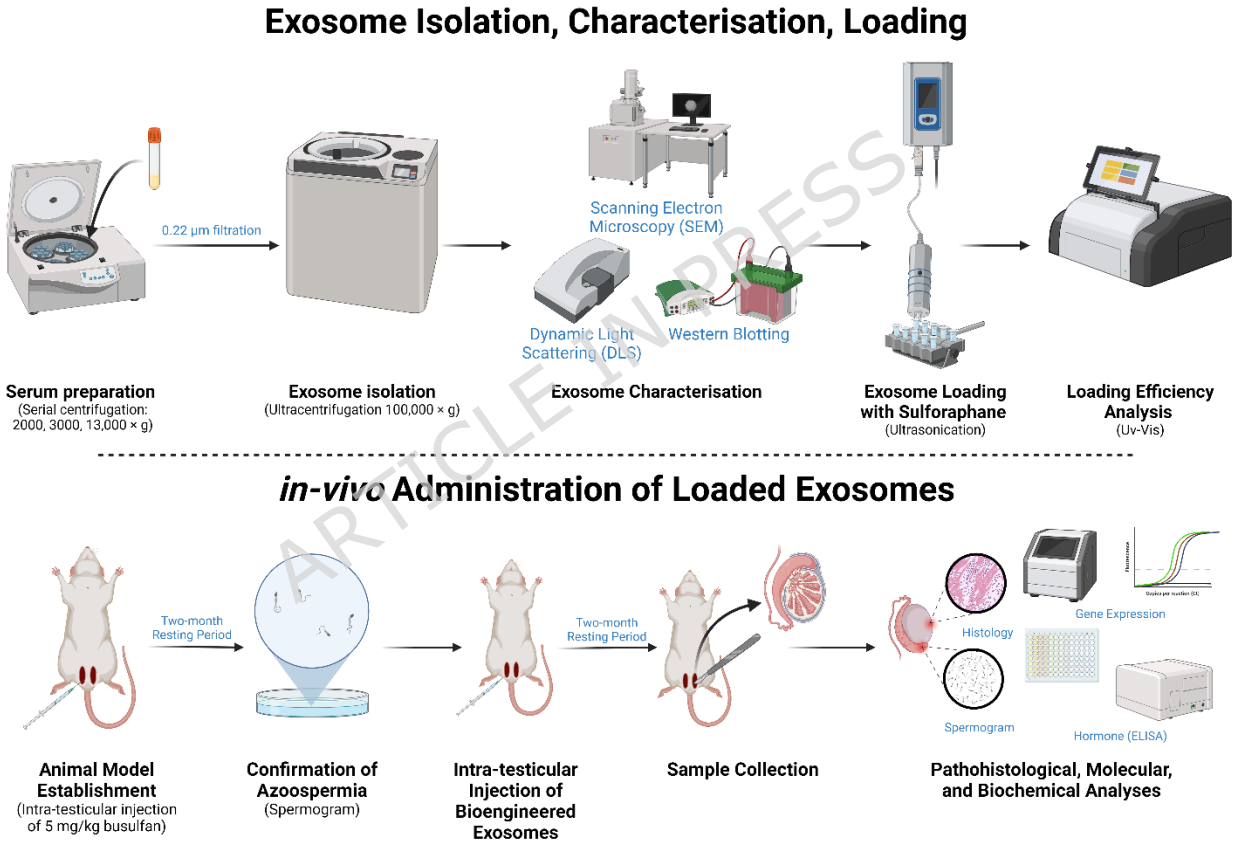

Figure 1. Illustration schematic processes of the current study. Exosomes were isolated and loaded with SFN, then, injected to busulfan-induced azoospermia rats. Following, supplementary examinations were performed to evaluate the therapeutic efficacy of SFN+EXO.

2. Materials and Methods

2.1 Exosome Isolation and Storage

Daily fresh human sera negative for common infections (e.g., HIV, HCV, HBV and syphilis) were collected from the Tabriz branch of Iranian Blood Transfusion Organization and immediately stored at -80°C until processing (19). After thawing, the sera (approximately 6 mL per isolation batch), were diluted 1:3 with PBS and then subjected to serial centrifugation at 4°C: 1500 g for 7 min, 5000 g for 10 min, for 13000 g for 30 min, followed by filtration through a 0.22 µm syringe filter. Sera were subsequently ultracentrifuged at 100,000 g for 1 h at 4°C and the pellet containing packed exosomes was dissolved in 200 µL of filtered PBS (5). Freshly isolated exosomes were stored at -80°C until use.

2.2 Exosome Characterization and Qualification

2.2.1 Dynamic Light Scattering

To determine the particle size distribution and zeta potential, the exosome samples were analyzed using Dynamic Light Scattering (DLS) (Anton Paar Litesizer™ 500, Austria). Prior to analysis, the isolated exosomes were diluted in PBS (1:50) to reach an optimal concentration range (approximately 10 µg/mL) to prevent multiple scattering artifacts. The actual protein concentration of the exosome suspension was quantified using the Bicinchoninic Acid Assay (BCA) total protein assay kit, which is described in following sections. Finally, the size distribution and zeta potential were evaluated, applying a refractive index of 1.37 for exosomes and 1.33 for water in at least 3 consecutive runs.

2.2.2 Scanning Electron Microscopy

Scanning electron microscopy (SEM) was employed for qualitative visualization and confirmation of exosome isolation. First, freshly isolated exosomes were fixed by mixing with 2.5% glutaraldehyde (1:1) and incubated for 1 h at 4°C to preserve their natural morphology. After fixation, a small

aliquot (approximately 20 µL) of fresh exosomes was deposited onto pre-cleaned aluminum foil and left to dry at room temperature for 1 h. To dehydrate the samples, the aluminum foils were rinsed in a graded series of ethanol (30%, 50%, 70%, 90% and 100% twice) for 10 minutes each. Following dehydration, the samples were allowed to air-dry in a dust-free chemical cabinet. Next, a thin layer of gold was coated onto the dried deposits and morphology and size were examined in multiple fields using a high-resolution scanning electron microscope (SEM, TeScan-Mira III, Czech Republic).

2.2.3 Bicinchoninic Acid Assay

To quantify the total exosomal protein concentration, an aliquot of stored exosomes was gently thawed on ice and diluted 1:1 (v/v) with ice-cold radioimmunoprecipitation assay (RIPA) lysis buffer, containing protease and phosphatase inhibitors. The mixture was incubated on ice for 15 min and briefly vortexed at 5-minute intervals during incubation to enhance membrane disruption and lysis efficiency. Then, the samples were subjected to BCA analysis (BCA Protein Quantification Kit, Cat: A101251, Parstous, Iran) according to the provided protocol, using bovine serum albumin as the standard for calibration. Briefly, a working solution, which was a mixture of BCA and copper reagents (1:50, v/v), was added to lysed exosomes or standard samples. Then, the final mixture was incubated at 60°C for 1 h in a dry bath incubator (Major Science, MD-02N, Taiwan), followed by 562 nm absorbance assessment via a Multiskan MS microplate reader.

2.2.4 Western Blotting

To confirm the identity of the isolated exosomes, the expression of specific exosomal surface markers (CD63 and TSG101) was evaluated based on previously established protocol (5). Briefly, isolated exosomes were lysed by mixing with RIPA buffer at a 1:1 ratio and incubated on ice for 30 min. The lysates were then centrifuged at 14,000 g for 15 minutes at 4°C to remove insoluble material. A total of 20-40 µg of protein from the supernatant was separated by SDS-PAGE on 10-12% polyacrylamide gels and transferred onto

PVDF membranes. Membranes were blocked with 5% skimmed milk for 1 h at room temperature and then incubated overnight at 4°C with primary antibodies against exosomal markers TSG101 and CD63 (Santa Cruz Biotechnology, sc-7964 and sc-5275; both diluted 1:200 according to the manufacturer's recommendations). After washing with TBST, membranes were incubated for 1 h at room temperature with HRP-conjugated secondary anti-mouse IgG antibody (Santa Cruz Biotechnology, sc-516102). Protein bands were visualized using a chemiluminescence detection kit (Abcam, ab65623).

2.3 Exosome Engineering and Sulforaphane Entrapment

Isolated exosome was pooled and divided into: (i) 1 mg/ml exosome + 2 mM SFN (SFN+EXO group; Cat: FS27960, Biosynth, UK) and (ii) 1 mg/ml exosome + PBS in a total volume of 2 mL each. The mixtures were then subjected to probe sonication (20 kHz, 20% amplitude) for six cycles with 2 min intervals (30s on/30s off, 4s pulse/ 2s pause, ice cooled). After sonication, the sample was incubated for 1 h at 37°C to recover the exosomal membranes (22). Next, mixtures were ultracentrifuged at 100,000 g for 1 h at 4°C to remove the unloaded SFN. The supernatants were collected and the pellets were dissolved in 600 µL sterile PBS and stored at -80°C immediately until use. The theoretical indirect loading efficiency of sulforaphane into exosomes was determined using the UV-vis spectrometry method (Jasco V-730 UV-visible spectrophotometer, Japan). Supernatants from three preparations, including Exosome + SFN, Exosome + PBS (for background absorbance) and SFN + PBS (baseline absorbance), were analyzed at 237 nm, the characteristic absorbance peak of SFN. The amount of unencapsulated SFN remaining in the supernatant was calculated using the following formula:

$$\text{Free SFN in supernatant (\%)} = 100 \times \frac{\text{Abs(SFN + EXO) - Abs(Exosome + PBS)}}{\text{Abs(SFN + PBS)}}$$

The indirect loading efficiency was then calculated by subtracting this value from 100% and the results were expressed as a percentage of SFN loaded into the exosomes.

2.4 Animals

All animal experiments were conducted in accordance with institutional and international guidelines for the care and use of laboratory animals. The study protocol was reviewed and approved by the Research Ethics Committee of Tabriz University of Medical Sciences (Approval Code: IR.TBZMED.AEC.1401.084). Throughout the study, all animals were monitored for any complications, including post-injection infections, sudden weight loss, or signs of pain. Although no adverse effects were observed, an ethical protocol was established in accordance with animal care guidelines to euthanize and exclude any animal showing severe suffering. The work has been reported in line with the ARRIVE guidelines 2.0.

2.4.1 Establishment of Azoospermia Rat Models

A total of 35 approximately 3-month-old male Wistar rats weighing approximately 150 g were purchased from the Animal Centre of Medzist Company (Tehran, Iran) and housed in the Physiology Animal Laboratory at Tabriz University of Medical Sciences. The animals were maintained under standard conditions with a 12-hour light/dark cycle, controlled temperature (20-25°C) and relative humidity (40-60%), with free access to laboratory chow and water. Following a two-week acclimatization period, the rats were used for experimental procedures. The azoospermia rat models were created using our previously established protocol (5, 23). Briefly, 27 rats were randomly assigned for azoospermia induction and anesthetized using an intraperitoneal injection of Ketamine (90 mg/kg) and Xylazine (10 mg/kg). Before injection, the scrotal area was disinfected with 70% ethanol. Then, azoospermia was induced via a single intratesticular injection of Busulfan (5 mg/kg body weight; Milosun, NanoAlvand Company, Iran).

This intratesticular route was selected to maximize local germ cell depletion while minimizing the systemic toxicity and high mortality rates often associated with intraperitoneal Busulfan administration, as explicitly evaluated in our previous study (23). To confirm the successful induction of azoospermia prior to treatment, 60 days post-injection, semen analysis and histological examination of testicular tissue were performed in 3 randomly selected azoospermic and 3 non-treated healthy control rats. Following this validation, the remaining animals were randomly allocated into the experimental groups.

2.4.2 Grouping, Study Design, and Treatments

After azoospermia confirmation, the animals were divided into two untreated control groups: healthy controls (n=5) and azoospermic controls (n=6). In addition, three experimental groups were considered (n=6 each): (i) the SFN group, in which azoospermic rats received only approximately 8 µg per testis sulforaphane; (ii) the EXO group, (iii) treated with only exosomes (~20 µg total protein per testis); and (iv) the SFN+EXO group, which received exosomes loaded with sulforaphane (~20 µg total exosomal protein per testis contained approximately 8 µg SFN).

All treatments were administered by intratesticular injection at a volume of 100 µL per testis. Injections were performed under deep anesthesia using a combination of ketamine (90 mg/kg) and xylazine (10 mg/kg). Following treatment, animals were maintained for a 2-month recovery period to allow for tissue healing. At the end of the study, animals were anesthetized with the same ketamine-xylazine mixture and blood and testis samples were collected. For the blood collection, under irreversible anesthesia, blood sample was drawn via cardiac puncture, followed by neck dissection to ensure euthanization. All procedures were performed by trained veterinarian (Dr. M. Fajri) to minimize animal suffering. Then, Blood samples were allowed to clot at room temperature for 30 min, then centrifuged at 1500 × g for 15 min to

separate the serum. Serum samples were aliquoted and immediately stored at -80°C for hormone analysis.

2.5 Epididymal Sperm Quality and Spermogram Analysis

After euthanasia, epididymal sperm were collected by finely chopping the caudal epididymis in Medium-199 supplemented with 20% fetal bovine serum (FBS), followed by incubation at 37°C for 30-45 min. Sperm motility was assessed using a light microscope at 40× magnification by examining at least 200 sperm cells across five different fields. Morphology was evaluated by analyzing 200 sperm per slide. Sperm concentration was measured using a Neubauer hemocytometer.

2.6 Histopathology

Testicular tissues were fixed in 4% paraformaldehyde, processed through a graded alcohol dehydration series and embedded in paraffin blocks. Serial sections (5 µm) were rehydrated through xylene and descending alcohol concentrations and stained with either hematoxylin and eosin (H&E) for general histological evaluation or Masson's trichrome for connective tissue visualization. Stained sections were studied using a microscope (Labomed LX 300, USA) with a high-resolution camera (Tucsen MIchrome 16, China).

2.7 ELISA

Serum testosterone levels were quantified using a commercial ELISA kit (Monobind Inc., Cat: 3725-300, USA) following the manufacturer's protocol. In brief, 10 µL of serum samples or standards were combined with 50 µL of enzyme and 50 µL biotin conjugates in the provided streptavidin-coated 96-well plate and incubated for 1 h at room temperature. Following three washes with diluted buffer, 100 µL of substrate solution was added to each well. The enzymatic reaction was terminated after 15 minutes by adding the stop solution and absorbance was immediately measured at 450 nm using a microplate reader (Multiskan MS, Finland). For quantification, concentrations of analytes were determined from optical density (OD) values using a

four-parameter logistic model fitted to the standard curve by non-linear regression in Python.

2.8 Gene Expression Analysis

Total RNA was extracted from testicular tissues using Trizol reagent (MaxZol, Iran). RNA concentration and purity were assessed using a Nanodrop (ND-100 UV-vis spectrophotometer, Thermo Fisher Scientific, USA). Complementary DNA (cDNA) was synthesized using a cDNA synthesis kit (Zist Virayesh, Cat: ZV06010050, Iran). Quantitative real-time PCR (qPCR) was performed using SYBR Green Master Mix (Zist Virayesh, Cat: ZV03021250, Iran) on a real-time PCR system (Roche LightCycler 96, USA). The reaction mixture (14 µL total volume) contained 7 µL of SYBR Green Master Mix, 1 µL of cDNA template, 1 µM of each primer and nuclease-free water. The cycling program was an initial denaturation at 95°C for 10 min, followed by 40 cycles of 95°C for 15 sec, 60°C for 10 sec and 72°C for 10 sec. Additionally, a melt curve analysis was performed to confirm amplification specificity. Target genes, including *DAZL*, *VASA*, *NFE2L2* (*Nrf2*), *Becn1* (*Beclin1*), *Map1lc3b* (*LC3*) and *SQSTM1* (*P62*), were analyzed and ACTB (β-actin) served as the reference gene for normalization. Primer sequences were designed using Primer-BLAST (NCBI) and presented in Table 1. Relative gene expression was calculated using the $2^{-\Delta\Delta Ct}$ method.

Table 1. Primer Sequences Used for qRT-PCR

Gene (NCBI Accession)		***Primer Sequence (3' → 5')***	***Amplicon Size (bp)***
DAZL (NM_001413924)	F	ATCTGTGGACCGAAGCATACAG	140
	R	TAAGCACTGCCCGACTTCTT	
VASA (NM_001077647)	F	AATAGCACAAGAGGGGCTGT	115
	R	CATCAACTGGATTGGGAGCTTG	
	F	CATTTCAGTCGCTTGCCCTG	147

Nrf2 (NM_001399173)	R	GCCAAACTTGCTCCATGTCC	
Beclin1 (NM_053739)	F	GCCTAAAGAATGGAGGGGTCT	125
	R	TGAATGGTCACTCGGTCCAG	
LC3 (NM_022867)	F	GGACAGCACTGGCTGTGTAA	129
	R	GTGGGTGCCTACGTTCTGAT	
P62 (NM_001393884)	F	GGAAGCTGAAACATGGGCAC	129
	R	CAACCTCGATGCCCGACTC	
β-actin (NM_031144)	F	ATTGGTGGCTCTATCCTGGC	144
	R	AGAAAGGGTGTAAAACGCAGC	

2.9 Oxidative Stress Profile (SOD, GPx, MDA, TAC)

Superoxide Dismutase (SOD) activity was measured using a colorimetric kit (Randox Laboratories Ltd., Cat: SD 125, UK). Superoxide radicals were generated by a xanthine-xanthine oxidase system. Tissue samples were lysed in RIPA buffer on ice, centrifuged to remove cell debris and the supernatant was used for the test. The reaction mixture was prepared by mixing the sample with the reagents and absorbance was measured at 505 nm after 3 min. SOD activity was calculated using a standard curve and reported as units per milligram of protein. Oxidative stress markers were normalized to total protein concentration (per mg protein) to account for differences in cellular protein content across samples. Glutathione Peroxidase (GPx) activity was measured using a commercial kit (Randox Laboratories Ltd., Cat: RS 504, UK). Tissue samples were lysed with RIPA buffer on ice and centrifuged. The reaction was carried out at 340 nm and GPx activity was expressed as units per milligram of protein.

Malondialdehyde (MDA) levels were measured using the thiobarbituric acid reactive substances method. Tissue samples were lysed in RIPA buffer on ice and centrifuged to remove debris. A volume of 500 µL of the supernatant was mixed with 3 mL of 1% phosphoric acid and 1 mL of 0.67% TBA solution. After

vortexing, the mixture was heated in a boiling water bath for 45 min. Following cooling, 3 mL of n-butanol was added and the mixture was vortexed and centrifuged at 3000 rpm for 10 min. The absorbance of the upper phase was read at 532 nm. MDA concentration was calculated using a standard curve prepared from 1,1,3,3-tetramethoxypropane and expressed as nmol per milligram of protein.

Total antioxidant capacity (TAC) was measured using a commercial kit (Randox Laboratories Ltd., Cat: NX 2332, UK), which measures the total ability of antioxidants in the sample to block the formation of a colored radical. Tissue lysates prepared with RIPA buffer were centrifuged and the supernatants were used for analysis. The sample was mixed with reagents and hydrogen peroxide and the change in absorbance was recorded at 600 nm after 3 min.

2.10 Statistical Analysis

All statistical analyses were performed using GraphPad Prism 10.3. For comparisons between two groups, an unpaired Student's *t*-test was applied and for three or more groups, a one-way ANOVA was conducted, followed by Tukey's post hoc test for multiple comparisons. Before performing parametric tests, the normal distribution of data was assessed using the Shapiro-Wilk test, and homogeneity of variances was verified with Brown-Forsythe test. Data are presented as mean ± SEM and statistical significance was set at $p < 0.05$.

3. Results

3.1 Exosome Isolation, Characterization, and Loading

Dynamic light scattering analysis indicated that the exosomes had a mean diameter of 61.17 ± 12.99 nm and their average zeta potential was measured at -11.4 mV (**Figure 2A, B**). Western blot analysis confirmed the presence of exosomal surface markers CD63 and TSG101 (**Figure 2C**). SEM further confirmed the characteristic round-shaped, nano-sized morphology of the exosomes, consistent with the size distribution observed in the DLS results

(**Figure 2D**). Sulforaphane was loaded into exosomes using ultrasonication, followed by ultracentrifugation to remove unencapsulated drug. DLS showed a moderate size increase in sulforaphane-loaded exosomes (mean after loading: 186.92 ± 50.23 nm) (22, 24-26). UV-vis analysis confirmed an indirect loading efficiency of approximately 47% (**Figure 2E, F**).

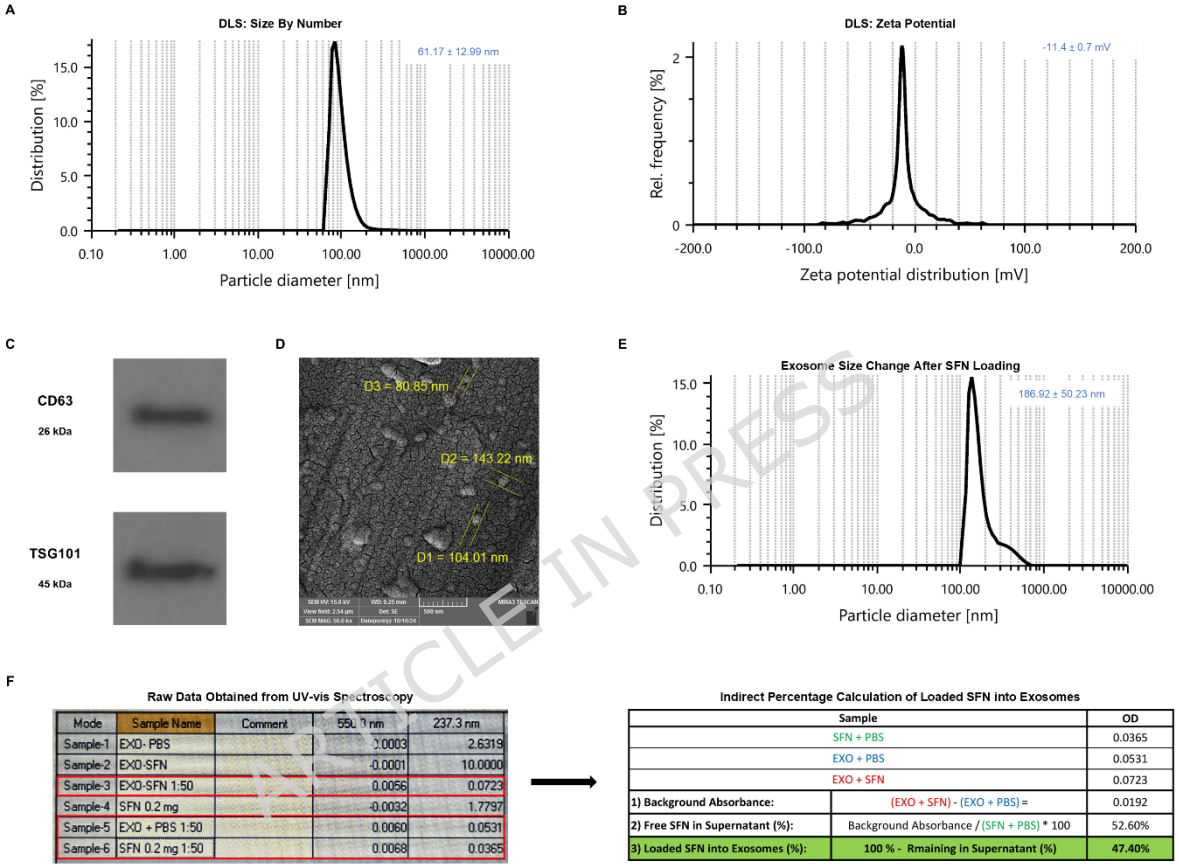

Figure 2. Characterization of human serum-derived exosomes and sulforaphane-loaded exosomes (SFN+EXO). (A, B) Dynamic light scattering (DLS) analysis indicates a particle size and zeta potential distribution centered around 61.17 nm and -11.4 mV, respectively. (C) Western blot analysis confirming the presence of exosomal markers CD63 and TSG101. (D) Scanning electron microscopy showing in range of sizes of round-shaped exosomes. (E) DLS analysis showing modest size change after SFN loading. (F) Sulforaphane loading efficiency determined by UV spectrophotometry.

3.2 SFN+EXO Significantly Restored Spermogram Parameters

Epididymal fluid sperm analysis at the time of testis collection revealed significant changes following both busulfan and sulforaphane-loaded exosome injections. Before treatment, the azoospermic rat model was confirmed by significantly reduced sperm count, percentage of morphologically normal sperms and sperm motility compared to healthy control. After treatment, significant differences were observed among groups in all assessed parameters as described below.

3.2.1 Sperm Count

The azoospermia group showed a significantly lower epididymal sperm count compared to the control group ($p = 0.0009$) before treatment intervention (**Figure 3A**). After treatment, the sperm count in the azoospermia group remained significantly lower than the control group ($p < 0.0001$). Treatment with SFN+EXO significantly improved sperm count compared to the azoospermia group ($p = 0.0012$). Similarly, both SFN-alone and EXO-alone increased sperm count, but these increases were not statistically significant when compared to azoospermia ($p > 0.4$). The combination treatment or SFN+EXO also showed significant improvements over SFN-alone ($p = 0.0011$) and EXO-alone ($p = 0.0224$) (**Figure 3A**).

3.2.2 Percentage of Morphologically Abnormal Spermatozoa

Before treatment, the percentage of morphologically abnormal spermatozoa was significantly higher in the azoospermia group (90.40%) compared to controls (2.42%) ($p < 0.0001$), confirming successful model establishment. After treatment, significant differences in percentages of abnormal spermatozoa were observed among all groups ($p < 0.0001$; **Figure 3B**). The azoospermia group retained a high abnormality rate (99.50%), which was not significantly improved by SFN alone (96.20%, $p = 0.9895$). In contrast, treatment with EXO (66.33%) and SFN+EXO (55.75%) significantly reduced the percentage of abnormal spermatozoa compared to the azoospermia group

(p = 0.0064 and p = 0.0002, respectively). SFN+EXO also resulted in significantly lower abnormality than SFN alone (p = 0.0003) and EXO alone (p = 0.0103), although the difference between EXO and SFN+EXO was not statistically significant (p = 0.6892; **Figure 3B**). These results indicate that sulforaphane-loaded exosomes effectively reduced sperm morphological abnormalities in azoospermic rats, with better outcomes compared to either sulforaphane or exosome treatment alone.

3.2.3 Sperm Motility

Sperm motility was significantly reduced in the azoospermia group compared to controls ($p < 0.0001$; **Figure 3C**). After treatment, SFN+EXO treatment significantly improved motility compared to azoospermia ($p < 0.0001$), while SFN-alone did not show significant improvement ($p = 0.5593$). Both SFN and EXO treatments were significantly different from SFN+EXO ($p = 0.0012$ and $p = 0.0050$, respectively). No significant differences were found between SFN and EXO groups ($p = 0.9931$; **Figure 3C**).

3.2.4 Testis Weight Index

Testicular weight was monitored as a gross anatomical indicator of spermatogenic status. Before treatment, the testis weight index was significantly lower in the azoospermia group compared to the control group ($p = 0.0027$), confirming successful establishment of the azoospermic rat model (**Figure 3D**). All groups showed a significant decrease in testis weight index compared to the control group ($p < 0.0001$) following treatment intervention. Among the treated groups, the SFN+EXO treatment significantly increased testis weight index compared to azoospermia alone ($p < 0.0001$). No significant difference was found between the azoospermia group and the SFN or EXO alone groups ($p = 0.7721$ and $p = 0.0631$, respectively). Additionally, SFN+EXO treatment showed significantly higher testis weight index compared to SFN alone ($p < 0.0001$) and EXO alone ($p = 0.0003$) (**Figure 3D**).

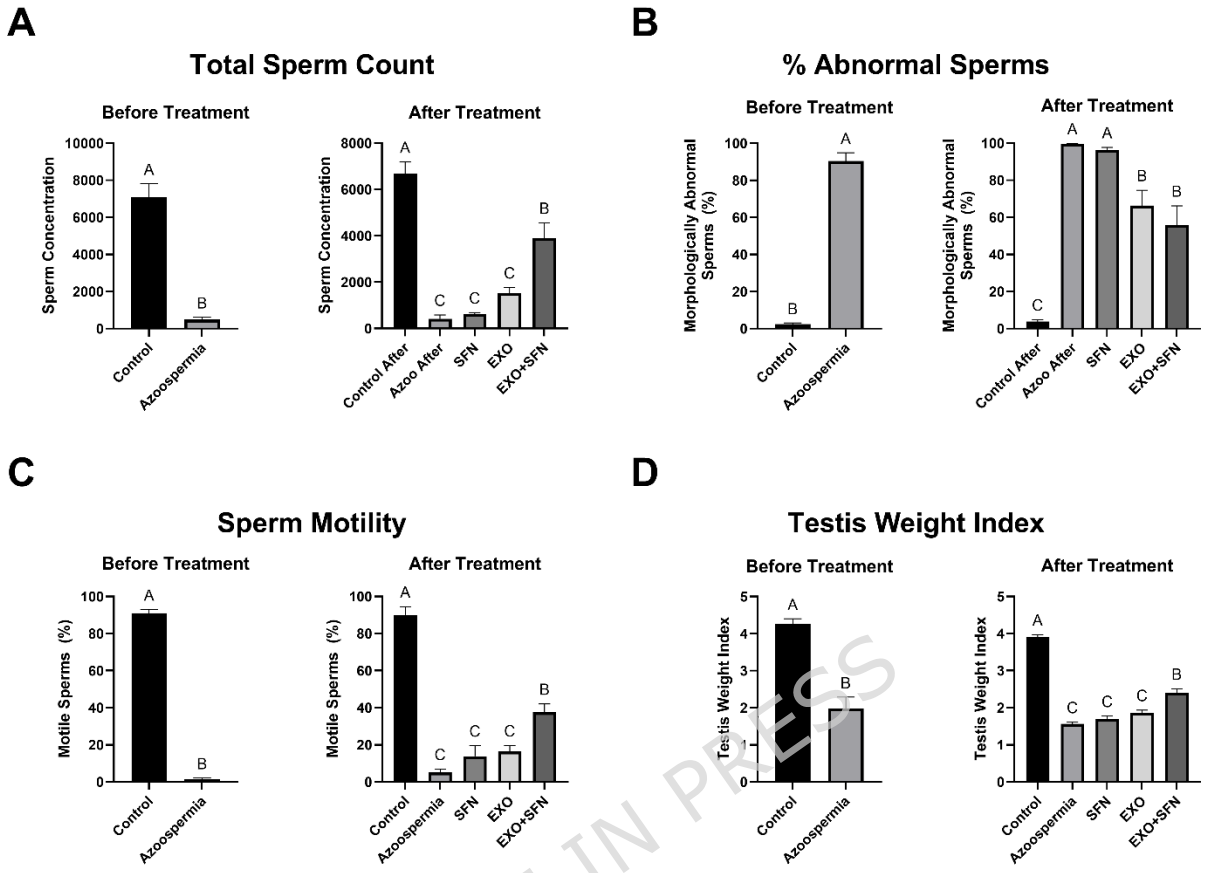

Figure 3. Epididymal spermogram parameters and testis weight index among different groups. Rats were assigned to control, azoospermia, SFN, EXO and SFN+EXO groups. (A) Total epididymal sperm count. (B) Percentage of morphologically abnormal sperms. (C) Percentage of motile spermatozoa. (D) Testis weight index (testis weight to body weight ratio). Data are presented as mean ± SEM.

3.3 SFN+EXO Attenuated Pathological Remodeling in Azoospermia Rats

Histological analysis revealed severe spermatogenic disruption in the busulfan-induced azoospermia group. Quantitative assessments confirmed that this model led to a notable depletion of all germ cell stages. Significant reductions in spermatogonial stem cells (SSCs), spermatocytes (SPCs) and

elongated spermatids (SPTs) were observed in the azoospermia group compared to healthy controls ($p < 0.0001$ for all comparisons; **Figure 4A-C**). Following therapeutic interventions, significant differences were observed across groups. SFN+EXO treatment resulted in markedly improved spermatogenic recovery across all germ cell types. SSCs in the SFN+EXO group were significantly higher than those in the azoospermia, SFN-only and EXO-only groups ($p < 0.05$ for all), although still lower than healthy controls ($p = 0.00025$; **Figure 4A**).

For SPCs, SFN+EXO restored counts to levels statistically very similar to the control group ($p > 0.1$), whereas SFN and EXO alone only partially improved SPC numbers and did not differ significantly from each other ($p = 0.8981$; **Figure 4B**). The most substantial improvement was observed in SPTs recovery in the SFN+EXO group. EXO was significantly more effective than SFN ($p < 0.0001$), underscoring the advantage of exosome-mediated delivery, especially in promoting late-stage germ cell maturation (**Figure 4C**). Together, these data demonstrate that SFN+EXO not only mitigates germ cell loss caused by chemotherapeutic insult but also fosters robust spermatogenic regeneration across multiple developmental stages, offering a promising therapeutic avenue for azoospermic infertility.

Histopathological evaluation demonstrated that SFN+EXO markedly preserved testicular tissue structure and mitigated pathological damage following chemically induced azoospermia (**Figure 4D, E**). In untreated azoospermic animals, seminiferous tubules showed extensive degeneration, germ cell loss, nuclear pyknosis and widespread hyaline necrosis. The interstitial space exhibited severe collagen deposition and architectural disruption, as confirmed by Masson’s trichrome staining, indicating advanced fibrosis. In contrast, SFN+EXO treatment substantially improved tissue integrity, with a visible increase in spermatogenic cells, reduced cellular necrosis and preserved tubular organization. The interstitium remained free of thickening or hyperemia and inflammation was minimal (**Figure 4D, E**).

Control tissues displayed intact spermatogenesis (all germ cell stages present) and minimal collagen restricted to basal laminae. SFN+EXO treatment compared to SFN and EXO groups achieved more consistent protection, evidenced by lower collagen accumulation and better restoration of spermatogenic activity. While the SFN group showed partial regeneration with persistent focal damage and moderate fibrosis and the unloaded exosome group exhibited uneven and incomplete recovery, SFN+EXO-treated tissues showed minimal fibrosis limited to the basal layer and nearly normal testicular architecture. These results highlighted the enhanced antifibrotic and regenerative effects of SFN+EXO, supporting its therapeutic potential in promoting fertility and testicular health after gonadotoxic injury (**Figure 4D, E**).

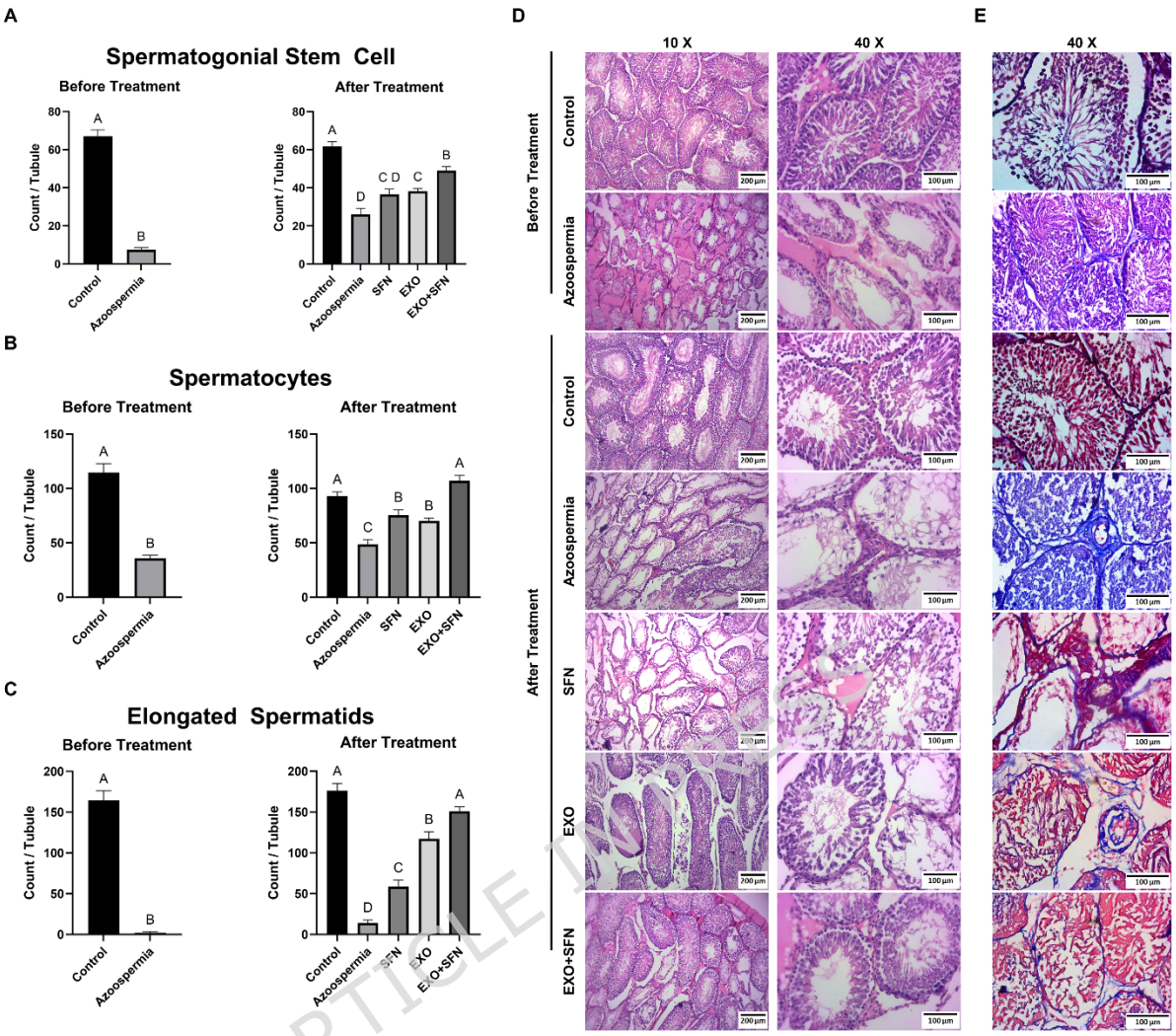

Figure 4. Histological evaluation of spermatogenesis recovery in busulfan-induced azoospermic rats following SFN, EXO and SFN+EXO treatments. (A-C) Quantification of spermatogonial stem cells, spermatocytes and elongated spermatids per seminiferous tubule. (D) Representative H&E-stained sections showing seminiferous tubule structure. (E) Masson's trichrome staining illustrating collagen deposition and interstitial fibrosis. Scale bars are indicated. Data are presented as mean ± SEM.

3.4 SFN+EXO Increased Testosterone Levels in Azoospermia Rats

To assess endocrine recovery following treatment, serum testosterone levels were measured using ELISA. In untreated azoospermic animals before treatment, testosterone levels significantly dropped (control: 5.818 ng/mL, azoospermia: 1.997 ng/mL, p = 0.0033; **Figure 5**). In post-intervention experimental groups, rats treated with SFN+EXO exhibited the highest testosterone levels, with a mean concentration of 3.311 ng/mL. In comparison, the azoospermic group showed markedly lower levels (2.478 ng/mL), while the sulforaphane-only (SFN: 3.078 ng/mL) and unloaded exosome (EXO: 3.019 ng/mL) groups demonstrated intermediate values (**Figure 5**). Statistical analysis revealed an increase in testosterone in the SFN+EXO group compared to the azoospermic group (p=0.0482) and no other comparisons reached a level of significance (**Figure 5**). These findings suggest that SFN+EXO treatment more effectively restores steroidogenesis than either sulforaphane or exosomes alone, highlighting the combinatorial approach's potential to support hormonal recovery in azoospermia.

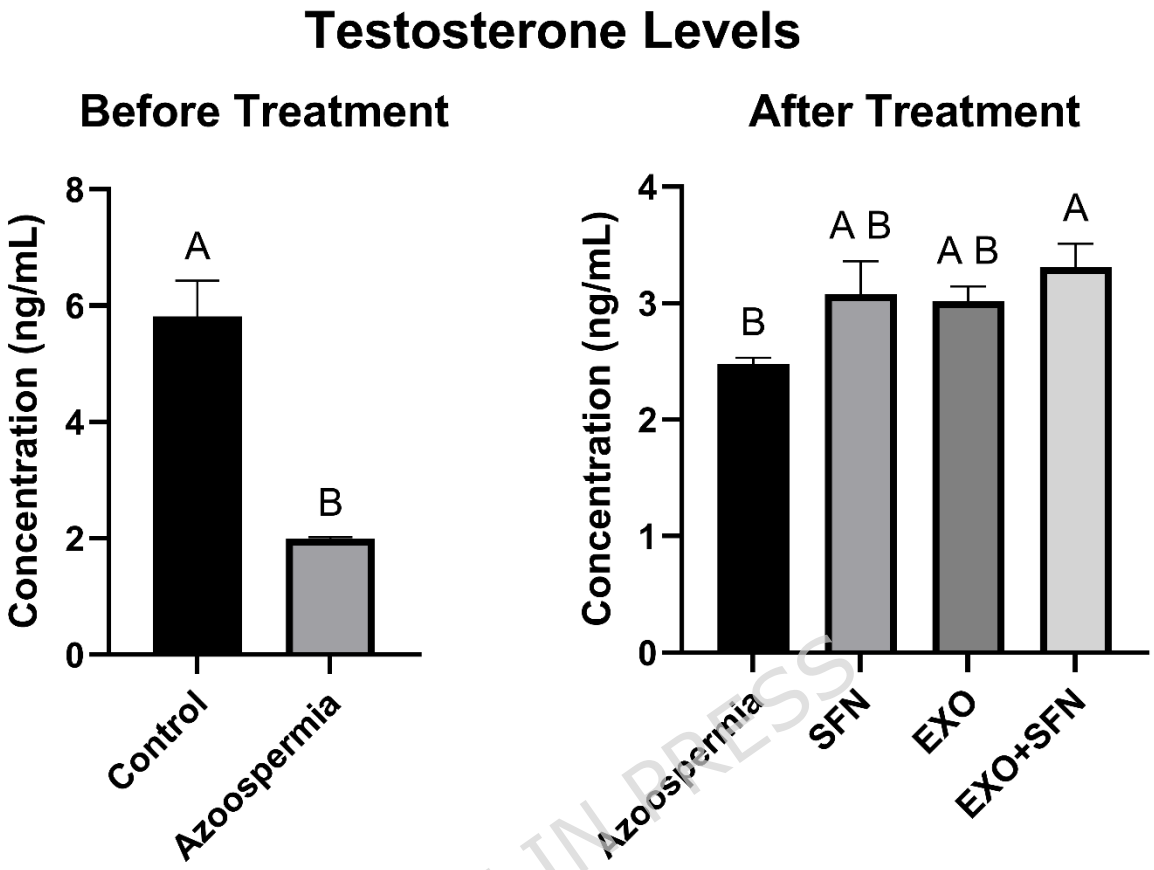

Figure 5. Effect of SFN-loaded exosomes on serum testosterone levels. Serum testosterone concentrations were quantified using ELISA to assess endocrine recovery. Data are presented as mean ± SEM.

3.5 SFN+EXO Up-regulated Spermatogenesis via Autophagy Activation

3.5.1. Spermatogenesis Markers (DAZL & VASA)

qRT-PCR results revealed that, the expression of both *DAZL* and *VASA* transcript was notably downregulated in the azoospermia model. After treatment, only the SFN+EXO combination fully restored expression to control levels for both *DAZL* (no difference vs. control, $p = 0.6226$) and *VASA* (no difference vs. control, $p > 0.9999$) and each was significantly higher than in

untreated azoospermia (*DAZL*, $p = 0.0187$; *VASA*, $p = 0.0415$). SFN- or EXO-alone produced partial, but incomplete, recovery of these markers (*DAZL*: $p = 0.0314$ and 0.0461; *VASA*: $p = 0.0894$ and 0.1402, respectively; **Figure 6A, B**).

3.5.2. Oxidative Stress Marker, Nrf2 Expression

Nrf2 is the master regulator of cellular antioxidant defenses and the primary target of our intervention. In the azoospermia model, *Nrf2* gene expression was significantly elevated at baseline ($p = 0.0381$), reflecting oxidative imbalance. Post-treatment, EXO and SFN+EXO both normalized *Nrf2* expression to nearly control levels (no difference vs. control, $p = 0.9811$ and 0.8799) and were significantly lower than untreated azoospermia ($p = 0.0215$ and 0.0025). SFN alone did not achieve a significant effect ($p = 0.3926$) (**Figure 6C**).

3.5.3. Autophagy Markers (LC3, Beclin1 & p62)

The transcriptional level of *Beclin1* (autophagy initiation factor), *LC3* (autophagosome membrane protein) and *p62* (selective autophagy adaptor) were all up-regulated in the azoospermia model (*LC3*, $p = 0.0129$; *Beclin1*, $p = 0.0372$; *p62*, $p = 0.0014$). Following treatment, SFN+EXO normalized each marker back to control levels (no difference vs. control for *LC3* and *p62*, $p > 0.999$; *Beclin1*, $p = 0.9598$) and significantly reduced them versus untreated azoospermia (*LC3*, $p = 0.0142$; *Beclin1*, $p = 0.0003$; *p62*, $p = 0.0222$). SFN alone also lowered, *LC3* ($p = 0.0308$), Beclin1 ($p = 0.0011$) and p62 ($p = 0.0343$) and EXO alone reduced *Beclin1* ($p = 0.0002$) and p62 ($p = 0.0265$; **Figure 6D-F**).

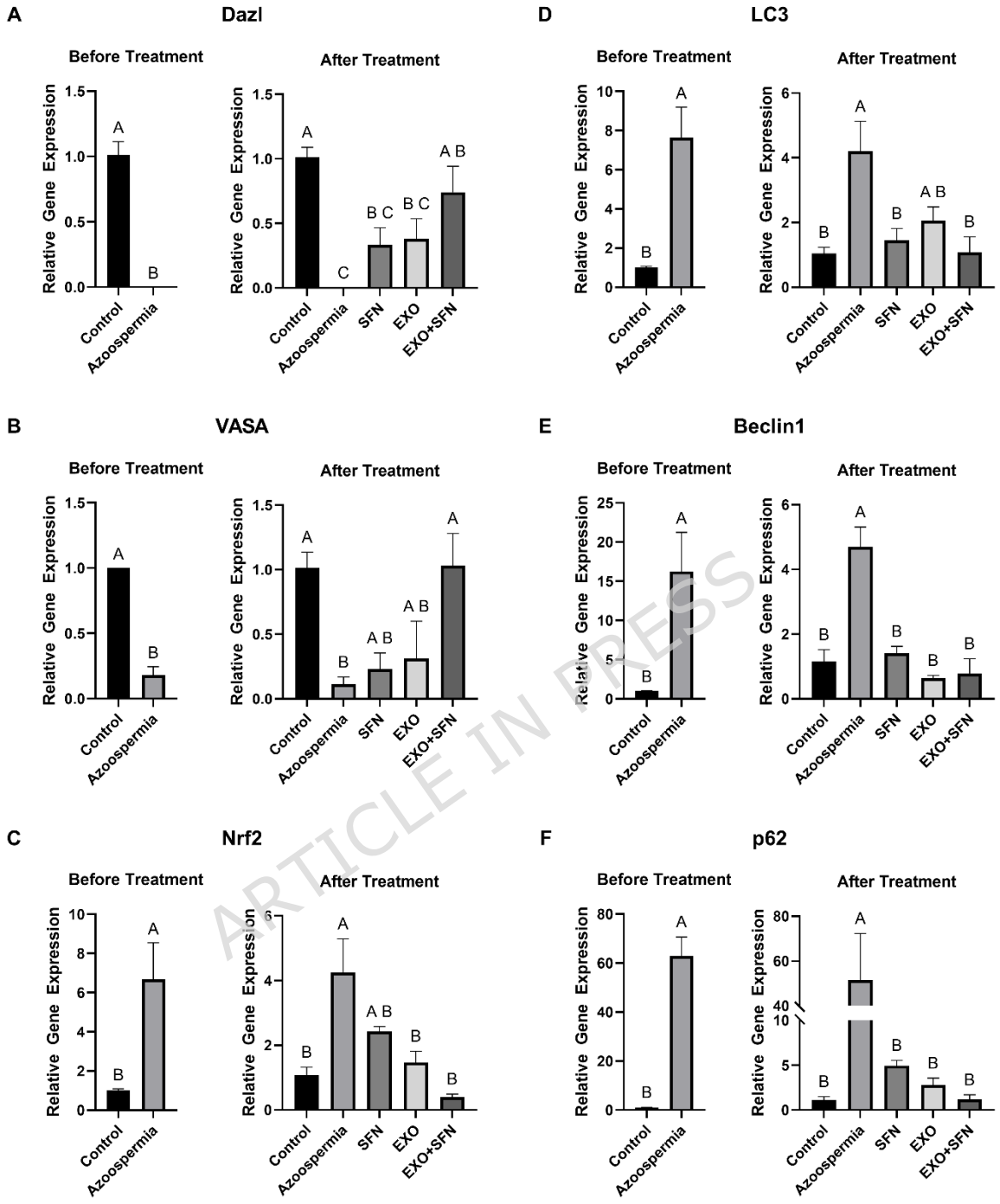

Figure 6. Relative gene expression of spermatogenesis (*DAZL* and *VASA*), *Nrf2* and autophagy-related genes (*LC3*, *Beclin1* and *p62*) in testicular tissue. qRT-PCR relative gene expression analysis of (A) *DAZL*, (B) *VASA*, (C) *Nrf2*, (D) *LC3*, (E) *Beclin1*, and (F) *p62* in control, azoospermic and treated groups. *β*-

actin was used as an internal control gene for normalization. Data are presented as mean ± SEM.

3.6 SFN+EXO modulated oxidative stress within the testicular tissues

To investigate the impact of SFN-loaded exosomes on oxidative stress in the testes, we measured malondialdehyde (MDA), glutathione peroxidase (GPx), superoxide dismutase (SOD) and total antioxidant capacity (TAC) expression across experimental groups. Lipid peroxidation, as indicated by MDA levels, showed no statistically significant differences among groups ($p > 0.05$). Notably, MDA levels did not significantly differ between the azoospermic group and any treatment groups (**Figure 7A**). This suggested that MDA levels were not substantially altered by either condition or treatment.

In contrast, GPx activity revealed significant improvements in antioxidant response, particularly in the SFN+EXO group. Compared to the control group, GPx activity was significantly lower in both EXO ($p = 0.0249$) and SFN+EXO ($p = 0.0005$) groups. The SFN+EXO group also showed a significant increase in GPx levels relative to the azoospermia group ($p = 0.0259$), indicating a partial restoration of antioxidant enzyme function. No significant differences were observed between the azoospermic and SFN-alone groups ($p = 0.9857$), suggesting that SFN alone had a limited effect on GPx activity in vivo (**Figure 7B**). While the mean values for SOD slightly increased in the treatment groups, these changes were not statistically meaningful ($p > 0.05$) (**Figure 7C**).

Interestingly, TAC showed a modest but significant increase in the SFN+EXO group compared to controls ($p = 0.0037$), suggesting a synergistic enhancement of systemic antioxidant capacity by the combined treatment. However, comparisons between other groups (e.g., SFN vs. SFN+EXO or EXO vs. EXO+SFN) remained statistically non-significant (**Figure 7D**). These findings indicate that while lipid peroxidation levels (MDA) remained unaffected, antioxidant defense systems, particularly GPx and TAC, were

modulated positively by exosome-based delivery of sulforaphane, with the combination treatment yielding the most notable improvements.

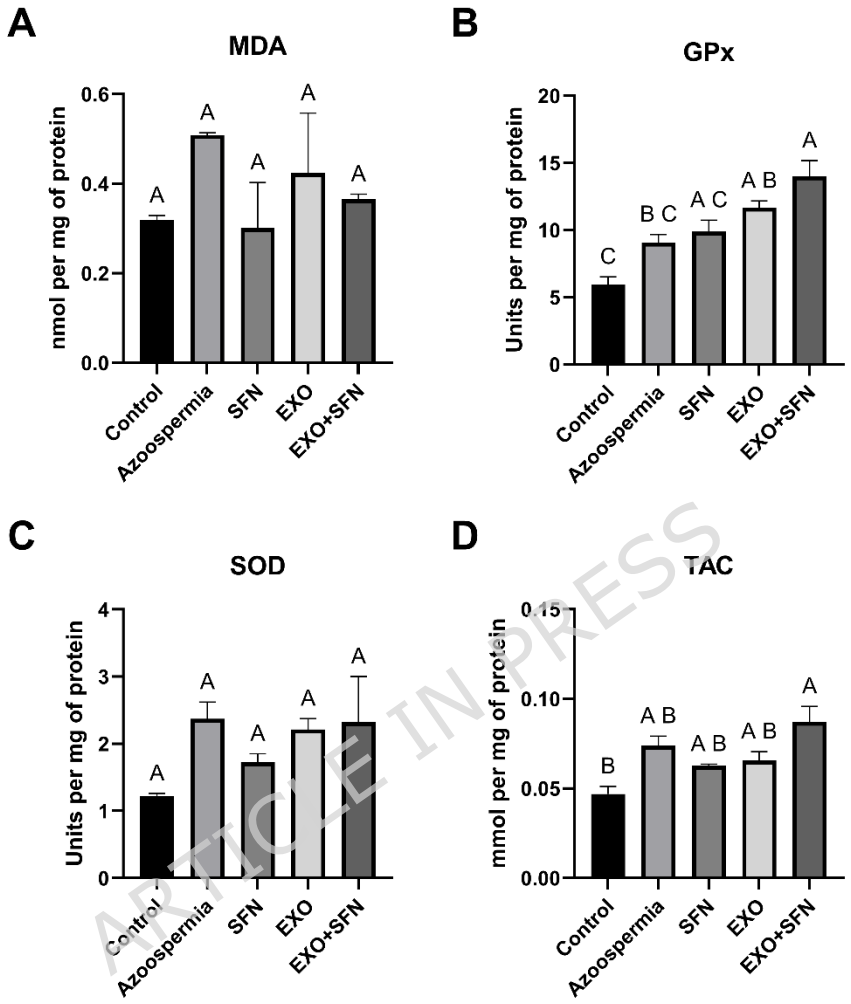

Figure 7. Evaluation of testicular oxidative stress profile post-treatment. The levels of (A) malondialdehyde (MDA), (B) glutathione peroxidase (GPx), (C) superoxide dismutase (SOD) and (D) total antioxidant capacity (TAC). Data are presented as mean ± SEM.

4. Discussion

Here, we indicated that the injection of SFN+EXO significantly restored spermatogenesis in our rat model of busulfan-induced azoospermia. Compared to untreated rats, SFN+EXO improved several sperm parameters,

such as count, morphology and motility, with concomitant increase of the testis weight index compared to SFN and EXO groups. The significant reduction in testis weight following Busulfan treatment reflects the massive depletion of germ cells and atrophy of seminiferous tubules. Conversely, the restoration of testicular weight in the SFN+EXO treated group correlates with the histological recovery and repopulation of the tubules.

Histological analysis showed severe loss of SSCs, SPCs and SPTs in azoospermic rats, while SFN+EXO significantly increased all three cell types, especially SPTs. These features were accompanied by the reduction of fibrotic changes evaluated by Masson's trichrome staining. These data confirmed the reduced interstitial fibrosis and preservation of seminiferous tubules in SFN+EXO rats. Interestingly, a single SFN+EXO dose had only mild fibrosis remained. It should be noted that while the Busulfan model is used to mimic azoospermia, it often results in a state of reversible azoospermia rather than the absolute absence of sperm. However, the statistically significant improvements in sperm count and motility in the SFN+EXO group clearly demonstrate the regenerative efficacy of the treatment compared to untreated controls.

At the molecular level, SFN+EXO fully restored *DAZL* and *VASA* gene expression levels, which are two key spermatogenesis markers, while monotherapies achieved partial recovery. We noted that the *Nrf2* transcription levels were elevated in azoospermic rats, while administration of EXO, SFN and/or SFN+EXO reduced these increased levels. While *Nrf2* activation and autophagy are protective during stress, their prolonged and persistent overexpression may reflect unresolved damage (27-29). Here, we showed that while both SFN and SFN+EXO significantly modulated autophagy pathways, the combination therapy (SFN+EXO) achieved a full restoration of spermatogenesis markers (*DAZL*, *VASA*) and higher functional recovery in sperm parameters, which highlights its enhanced efficacy. The upregulation of autophagy-related genes and normalization of Nrf2 expression in the

SFN+EXO group suggest that this therapeutic benefit may involve in activation of autophagy flux and antioxidant pathways. However, as no intervention trials (e.g., using autophagy or Nrf2 inhibitors) have been performed, this hypothesis remains plausible and requires direct validations in future studies.

Nrf2 activation induces antioxidant enzymes such as glutathione peroxidases to scavenge ROS (30). However, constant high *Nrf2* gene expression levels, as observed in untreated azoospermia, could indicate an imbalance in redox homeostasis, persistent oxidative stress and disrupted normal cell functions (31-34). *Nrf2* activation may also drive stem/progenitor cells out of quiescence, leading to premature differentiation and depletion of the stem cell pool (35-38). For instance, in an experiment, it was suggested that prolonged *Nrf2* activity impairs quiescence and regenerative capacity of hematopoietic stem cells (36, 38). In the context of our model, we hypothesize that sustained high levels of Nrf2, as observed in untreated azoospermia, may drive SSCs out of their protective quiescent state and into premature differentiation. This forced exit from the stem cell pool, without adequate replacement, could lead to the gradual decline of SSCs. Thus, the histological loss of cells may be the result of this aberrant differentiation caused by persistent Nrf2 activation, rather than immediate cell death. The relationship between the *Nrf2* activation and specific regulatory pathways requires further investigation.

While physiological levels of autophagy help remove damaged mitochondria and misfolded proteins, its overactivation might be detrimental and trigger apoptosis (39-41). In the testicular tissue, constant activation of autophagy might disrupt the function of both germ cells and supporting cells, which potentially affects the tissue’s regenerative capacity (42). In the present study, increased *p62* transcriptional levels observed in untreated azoospermia may indicate disrupted autophagy, possibly due to impaired lysosomal degradation, resulting in cellular waste accumulation and increased germ cell loss (43-45). In a previous experiment by our research group, human amniotic fluid-derived exosomes increased expression of SSC markers (OCT3/4, DAZL,

VASA) and improved testicular histology in azoospermic rats (5). Along with these findings, other studies have proven that umbilical cord- and adipose- and urine-derived mesenchymal stem cell exosomes can also alleviate busulfan-induced azoospermia in rodent models, promote germ cell proliferation in vitro and partially restore sperm counts in vivo (46-48). Of note, the injection of naïve exosomes provided only modest reparative effects compared to SFN+EXO. Based on our data, SFN+EXO yielded significantly superior molecular and functional modulation of autophagy.

Nrf2 activation via KEAP1 knockdown in mouse liver has been demonstrated to cause AKT-driven hepatomegaly and early fibrosis, indicating Nrf2's role in pathogenic remodeling (49). Therefore, it is assumed that the extensive collagen deposition in untreated azoospermic testes may, at least in part, be related to sustained Nrf2 activity leading to fibrosis. Notably, SFN+EXO treatment effectively normalized Nrf2 expression to levels comparable with healthy controls and provided sufficient antioxidant defense to mitigate ROS without inducing Nrf2 overactivation. These findings underscore the importance of precisely regulating Nrf2 activity for effective tissue repair. The protective role of SFN through Nrf2 activation is well documented (50, 51).In a busulfan-induced oligospermia model, SFN treatment significantly improved sperm concentration and motility and upregulated testicular Nrf2 and GPX4 expression (52). Similarly, in a chemically-induced testicular toxicity model, SFN preconditioning ameliorated fibrosis, preserved seminiferous tubule structure and partially restored sperm count and motility via activation of the Nrf2/SLC7A11/GPX4 axis (53). Our findings extend this insight by showing that exosome-mediated SFN delivery more effectively restored both Nrf2 signaling and autophagic processes, resulting in more complete histological and functional recovery than SFN alone. Previous research has also linked increased autophagy to apoptosis. For example, in heat-induced testicular injury, upregulation of autophagy was accompanied by extensive germ cell apoptosis (42). Conversely, genetic inhibition of autophagy (e.g., Atg7

knockdown) reduced apoptosis and preserved spermatogenesis, suggesting that excessive autophagy can be harmful to germ cells (42). Similar observations have been made in ischemia-reperfusion injury and neurodegenerative diseases, where excessive autophagy leads to cell death and disease progression (54-57).

Although few studies have directly examined autophagy in the context of testicular regeneration, available evidence suggests that transient induction is protective, whereas chronic overactivation is detrimental. In a rodent heat-stress model, autophagy markers increased in parallel with apoptosis markers and, interestingly, inhibition of autophagy in that model reversed cell death and preserved SSCs (42). In this study, the persistent elevation in LC3, Beclin1 and p62 in untreated azoospermic rats indicates dysregulated autophagy. In contrast, SFN+EXO treatment normalized these markers to levels comparable to healthy controls. This suggests that normal autophagy turnover ultimately supported germ cell survival. Treatment with SFN+EXO restored spermatogenesis, expression of Nrf2 and autophagy-related markers to near-baseline levels, indicating a more regulated and balanced autophagic and antioxidant defense process. This may have supported the clearance of damaged cellular components, preserved the SSC niche and enhanced germ cell repopulation. These findings support the conclusion that precise modulation of oxidative stress and autophagy pathways is essential for effective testicular regeneration. The improved outcomes observed with SFN-containing exosomes highlight their potential as a targeted therapeutic strategy for male infertility. Moreover, this approach may offer broader applications in regenerative medicine, where maintaining stem cell integrity and tissue homeostasis is crucial.

Limitations and recommendations for future research

This study was limited to a two-month follow-up in a single azoospermia model (busulfan-induced), providing preliminary insights into the therapeutic potential of SFN+EXO for azoospermia recovery. Future research should

measure the loading efficiency of SFN+EXO with direct methods such as HPLC, optimize the dose and evaluate sperm viability alongside other sperm parameters, long-term fertility and safety outcomes in a larger sample size to further confirm the validity of the results. Mechanistic studies using autophagy inhibitors or Nrf2/Keap1 modulators and the interaction between Nrf2 and autophagy could clarify the therapeutic pathways. In addition, the fertility of treated rats and the health of offspring will need to be examined. These efforts will better define how SFN+EXO restores spermatogenesis through redox and autophagy regulation. Although exosome identity was confirmed using several complementary methods, the absence of negative markers in Western blot and SEM images after exosome bioengineering could limit the complete assessment of exosome purity and manipulations.

5. Conclusion

SFN-loaded exosome therapy supported testicular regeneration, possibly through modulation of cellular signaling from a chronic oxidative state toward physiological balance. This promoted the recovery of spermatogonial stem cell proliferation and differentiation, as indicated by the re-expression of germ cell-specific markers (DAZL, VASA) and increased sperm counts. The therapeutic effect was likely associated with the targeted delivery of SFN via bioengineered exosomes, which regulated Nrf2 homeostasis and autophagy to remove damaged cellular components. These findings suggest that regulation of these pathways could play important roles in supporting testicular regeneration. Further studies are needed to explore the long-term safety, dosing strategies and translational potential of SFN-loaded exosome therapy in reproductive medicine.

6. Abbreviations

SFN	Sulforaphane
EXO	Exosome
SFN+EXO	Sulforaphane-loaded exosome
Nrf2	Nuclear factor erythroid 2-related factor 2
ROS	Reactive oxygen species
SOD	Superoxide Dismutase
GPx	Glutathione Peroxidase
MDA	Malondialdehyde
TAC	Total antioxidant capacity
SSCs	Spermatogonial stem cells
SPCs	Spermatocytes
SPTs	Elongated spermatids

7. Acknowledgment

The authors would like to thank the Stem Cell Research Center and Core Research Laboratory, Tabriz University of Medical Sciences, for supporting this work. The graphical abstract was created with BioRender (www.biorender.com). The authors used an AI-assisted tool solely for language editing, grammar checking and writing style enhancement. No AI-generated content, data, or images were used in the preparation of this manuscript and the authors take full responsibility for the final text.

8. Authors' Contributions

S.A. performed all experiments, data analysis, graphical abstract design, data visualization and wrote the initial draft of the manuscript. M.F. participated in animal husbandry, treatments and H&E sperm counting. R.R performed pathological studies on H&E and Masson's trichrome slides. B.R, A.A., M.T. and

R.R reviewed and revised the initial draft of the manuscript. M.M. designed and conceptualized the project and the manuscript.

9. Funding

This study was supported by grants from Tabriz University of Medical Sciences and the Stem Cell Research Center (Grant Numbers: 70877 and 71978). It was also conducted as part of the Ph.D. research project of Shahin Ahmadian's dissertation titled "Studying the regenerative effects of engineered exosomes loaded with Nrf2 activator in the rat model of azoospermia". The project received ethical approval on February 13, 2023, from the Research Ethics Committee for Laboratory Animals at Tabriz University of Medical Sciences (Ethical Code: IR.TBZMED.AEC.1401.084).

10. Data Availability

All data obtained or analyzed during this study are included in this published article and the supplementary file.

Declarations

11. Ethics approval and consent to participate

All experimental protocols, under the Ph.D. project of Shahin Ahmadian title "Study of the restorative effects of engineered exosomes containing Nrf2 activator in a rat model with azoospermia," were approved by the Animal Ethics Committee of Tabriz University of Medical Sciences (approval number IR.TBZMED.AEC.1401.084; approval date: February 13, 2023). All animal procedures were performed in accordance with the ARRIVE 2.0 guidelines, relevant institutional regulations and national guidelines for the care and use

of laboratory animals. The human serum samples utilized in this project were remnants from routine screenings at the Iranian Blood Transfusion Organization. These samples were delivered to the laboratory in a completely anonymous manner, with no personal identifiers provided to the research team before the exosome extraction process. The ethics committee waived the requirement for informed consent for the use of these anonymous residual samples.

12. Consent for publication

Not applicable.

13. Competing interests

The authors declare that they have no competing interests.

14. References

1. Njagi P, Groot W, Arsenijevic J, Mburu G, Chambers G, Calhaz-Jorge C, et al. Financial cost of assisted reproductive technology for patients in high-income countries: A systematic review protocol. PLoS One. 2025;20(2):e0318780.

2. Corona G, Minhas S, Giwercman A, Bettocchi C, Dinkelman-Smit M, Dohle G, et al. Sperm recovery and ICSI outcomes in men with non-obstructive azoospermia: a systematic review and meta-analysis. Hum Reprod Update. 2019;25(6):733-57.

3. Esteves SC, Achermann APP, Miyaoka R, Verza S, Jr., Fregonesi A, Riccetto CLZ. Clinical factors impacting microdissection testicular sperm extraction success in hypogonadal men with nonobstructive azoospermia. Fertil Steril. 2024;122(4):636-47.

4. Tharakan T, Corona G, Foran D, Salonia A, Sofikitis N, Giwercman A, et al. Does hormonal therapy improve sperm retrieval rates in men with non-obstructive azoospermia: a systematic review and meta-analysis. Hum Reprod Update. 2022;28(5):609-28.

5. Mobarak H, Heidarpour M, Rahbarghazi R, Nouri M, Mahdipour M. Amniotic fluid-derived exosomes improved spermatogenesis in a rat model of azoospermia. Life Sci. 2021;274:119336.

6. Aitken RJ, De Iuliis GN. On the possible origins of DNA damage in human spermatozoa. Mol Hum Reprod. 2010;16(1):3-13.

7. Aitken RJ, Baker MA. Oxidative stress, sperm survival and fertility control. Mol Cell Endocrinol. 2006;250(1-2):66-9.

8. Agarwal A, Virk G, Ong C, du Plessis SS. Effect of oxidative stress on male reproduction. World J Mens Health. 2014;32(1):1-17.

9. Takalani NB, Monageng EM, Mohlala K, Monsees TK, Henkel R, Opuwari CS. Role of oxidative stress in male infertility. Reprod Fertil. 2023;4(3).

10. Barati E, Nikzad H, Karimian M. Oxidative stress and male infertility: current knowledge of pathophysiology and role of antioxidant therapy in disease management. Cell Mol Life Sci. 2020;77(1):93-113.

11. Ma Q. Role of nrf2 in oxidative stress and toxicity. Annu Rev Pharmacol Toxicol. 2013;53:401-26.

12. Yamamoto M, Kensler TW, Motohashi H. The KEAP1-NRF2 System: a Thiol-Based Sensor-Effector Apparatus for Maintaining Redox Homeostasis. Physiol Rev. 2018;98(3):1169-203.

13. Cuadrado A, Rojo AI, Wells G, Hayes JD, Cousin SP, Rumsey WL, et al. Therapeutic targeting of the NRF2 and KEAP1 partnership in chronic diseases. Nat Rev Drug Discov. 2019;18(4):295-317.

14. Kensler TW, Wakabayashi N, Biswal S. Cell survival responses to environmental stresses via the Keap1-Nrf2-ARE pathway. Annu Rev Pharmacol Toxicol. 2007;47:89-116.

15. Liebman SE, Le TH. Eat Your Broccoli: Oxidative Stress, NRF2, and Sulforaphane in Chronic Kidney Disease. Nutrients. 2021;13(1):226.

16. Lu W. Sulforaphane regulates AngII-induced podocyte oxidative stress injury through the Nrf2-Keap1/ho-1/ROS pathway. Ren Fail. 2024;46(2):2416937.

17. Yuanfeng W, Chengzhi L, Ligen Z, Juan S, Xinjie S, Yao Z, et al. Approaches for enhancing the stability and formation of sulforaphane. Food Chem. 2021;345:128771.

18. Franklin SJ, Dickinson SE, Karlage KL, Bowden GT, Myrdal PB. Stability of sulforaphane for topical formulation. Drug Dev Ind Pharm. 2014;40(4):494-502.

19. Ahmadian S, Jafari N, Tamadon A, Ghaffarzadeh A, Rahbarghazi R, Mahdipour M. Different storage and freezing protocols for extracellular vesicles: a systematic review. Stem Cell Res Ther. 2024;15(1):453.

20. Mirzaahmadi B, Ahmadian S, Haddadi P, Nezhad-Mokhtari P, Nezamdoust FV, Yalameha B, et al. Neuroangiogenesis potential of mesenchymal stem cell extracellular vesicles in ischemic stroke conditions. Cell Commun Signal. 2025;23(1):272.

21. Zeng H, Guo S, Ren X, Wu Z, Liu S, Yao X. Current Strategies for Exosome Cargo Loading and Targeting Delivery. Cells. 2023;12(10).

22. Haney MJ, Klyachko NL, Zhao Y, Gupta R, Plotnikova EG, He Z, et al. Exosomes as drug delivery vehicles for Parkinson's disease therapy. J Control Release. 2015;207:18-30.

23. Mobarak H, Rahbarghazi R, Nouri M, Heidarpour M, Mahdipour M. Intratesticular versus intraperitoneal injection of Busulfan for the induction of azoospermia in a rat model. BMC Pharmacol Toxicol. 2022;23(1):50.

24. Zhuang J, Tan J, Wu C, Zhang J, Liu T, Fan C, et al. Extracellular vesicles engineered with valency-controlled DNA nanostructures deliver CRISPR/Cas9 system for gene therapy. Nucleic Acids Res. 2020;48(16):8870-82.

25. Kim MS, Haney MJ, Zhao Y, Yuan D, Deygen I, Klyachko NL, et al. Engineering macrophage-derived exosomes for targeted paclitaxel delivery to pulmonary metastases: in vitro and in vivo evaluations. Nanomedicine. 2018;14(1):195-204.

26. Nizamudeen ZA, Xerri R, Parmenter C, Suain K, Markus R, Chakrabarti L, et al. Low-Power Sonication Can Alter Extracellular Vesicle Size and Properties. Cells. 2021;10(9).

27. Jiang T, Harder B, Rojo de la Vega M, Wong PK, Chapman E, Zhang DD. p62 links autophagy and Nrf2 signaling. Free Radic Biol Med. 2015;88(Pt B):199-204.

28. Shan C, Wang Y, Wang Y. The Crosstalk between Autophagy and Nrf2 Signaling in Cancer: from Biology to Clinical Applications. Int J Biol Sci. 2024;20(15):6181-206.

29. Lau A, Wang XJ, Zhao F, Villeneuve NF, Wu T, Jiang T, et al. A noncanonical mechanism of Nrf2 activation by autophagy deficiency: direct interaction between Keap1 and p62. Mol Cell Biol. 2010;30(13):3275-85.

30. Ngo V, Duennwald ML. Nrf2 and Oxidative Stress: A General Overview of Mechanisms and Implications in Human Disease. Antioxidants (Basel). 2022;11(12).

31. Lian CY, Chu BX, Xia WH, Wang ZY, Fan RF, Wang L. Persistent activation of Nrf2 in a p62-dependent non-canonical manner aggravates lead-induced kidney injury by promoting apoptosis and inhibiting autophagy. J Adv Res. 2023;46:87-100.

32. Fan RF, Tang KK, Wang ZY, Wang L. Persistent activation of Nrf2 promotes a vicious cycle of oxidative stress and autophagy inhibition in cadmium-induced kidney injury. Toxicology. 2021;464:152999.

33. Romero-Duran MA, Silva-Garcia O, Perez-Aguilar JM, Baizabal-Aguirre VM. Mechanisms of Keap1/Nrf2 modulation in bacterial infections: implications in persistence and clearance. Front Immunol. 2024;15:1508787.

34. Rajasekaran NS, Varadharaj S, Khanderao GD, Davidson CJ, Kannan S, Firpo MA, et al. Sustained activation of nuclear erythroid 2-related factor 2/antioxidant response element signaling promotes reductive stress in the human mutant protein aggregation cardiomyopathy in mice. Antioxid Redox Signal. 2011;14(6):957-71.

35. Dai X, Yan X, Wintergerst KA, Cai L, Keller BB, Tan Y. Nrf2: Redox and Metabolic Regulator of Stem Cell State and Function. Trends Mol Med. 2020;26(2):185-200.

36. Murakami S, Suzuki T, Harigae H, Romeo PH, Yamamoto M, Motohashi H. NRF2 Activation Impairs Quiescence and Bone Marrow Reconstitution Capacity of Hematopoietic Stem Cells. Mol Cell Biol. 2017;37(19).

37. Murakami S, Shimizu R, Romeo PH, Yamamoto M, Motohashi H. Keap1-Nrf2 system regulates cell fate determination of hematopoietic stem cells. Genes Cells. 2014;19(3):239-53.

38. Tsai JJ, Dudakov JA, Takahashi K, Shieh JH, Velardi E, Holland AM, et al. Nrf2 regulates haematopoietic stem cell function. Nat Cell Biol. 2013;15(3):309-16.

39. Yan Q, Zhang Y, Wang Q, Yuan L. Autophagy: A Double-Edged Sword in Male Reproduction. Int J Mol Sci. 2022;23(23).

40. Liu Y, Levine B. Autosis and autophagic cell death: the dark side of autophagy. Cell Death Differ. 2015;22(3):367-76.

41. Liu S, Yao S, Yang H, Liu S, Wang Y. Autophagy: Regulator of cell death. Cell Death Dis. 2023;14(10):648.

42. Zhang M, Jiang M, Bi Y, Zhu H, Zhou Z, Sha J. Autophagy and apoptosis act as partners to induce germ cell death after heat stress in mice. PLoS One. 2012;7(7):e41412.

43. Liu WJ, Ye L, Huang WF, Guo LJ, Xu ZG, Wu HL, et al. p62 links the autophagy pathway and the ubiqutin-proteasome system upon ubiquitinated protein degradation. Cell Mol Biol Lett. 2016;21:29.

44. Kumar AV, Mills J, Lapierre LR. Selective Autophagy Receptor p62/SQSTM1, a Pivotal Player in Stress and Aging. Front Cell Dev Biol. 2022;10:793328.

45. Kageyama S, Gudmundsson SR, Sou YS, Ichimura Y, Tamura N, Kazuno S, et al. p62/SQSTM1-droplet serves as a platform for autophagosome formation and anti-oxidative stress response. Nat Commun. 2021;12(1):16.

46. Sheikholeslami A, Davoodi Asl F, Fazaeli H, Sheykhhasan M, Kalhor N, Naserpour L. Exosomes of mesenchymal stem cells and PRP restore spermatogenesis in the rat model of non-obstructive azoospermia. Reproduction. 2024;168(3).

47. Deng C, Xie Y, Zhang C, Ouyang B, Chen H, Lv L, et al. Urine-Derived Stem Cells Facilitate Endogenous Spermatogenesis Restoration of Busulfan-Induced Nonobstructive Azoospermic Mice by Paracrine Exosomes. Stem Cells Dev. 2019;28(19):1322-33.

48. Yue D, Wang F, Han Y, Xiong C, Yang R. Exosomes derived from umbilical cord mesenchymal stem cells ameliorate male infertility caused by busulfan in vivo and in vitro. Ecotoxicol Environ Saf. 2024;272:116063.

49. He F, Antonucci L, Yamachika S, Zhang Z, Taniguchi K, Umemura A, et al. NRF2 activates growth factor genes and downstream AKT signaling to induce mouse and human hepatomegaly. J Hepatol. 2020;72(6):1182-95.

50. Bai Y, Wang X, Zhao S, Ma C, Cui J, Zheng Y. Sulforaphane Protects against Cardiovascular Disease via Nrf2 Activation. Oxid Med Cell Longev. 2015;2015:407580.

51. Kubo E, Chhunchha B, Singh P, Sasaki H, Singh DP. Sulforaphane reactivates cellular antioxidant defense by inducing Nrf2/ARE/Prdx6 activity during aging and oxidative stress. Sci Rep. 2017;7(1):14130.

52. Zhao X, Liu Z, Gao J, Li H, Wang X, Li Y, et al. Inhibition of ferroptosis attenuates busulfan-induced oligospermia in mice. Toxicology. 2020;440:152489.

53. Elseweidy MM, Harb NG, Ali AA, El-Aziz RMA, Elrashidy RA. Sulforaphane substantially impedes testicular ferroptosis in adult rats exposed to di-2-ethylhexyl phthalate through activation of NRF-2/SLC7A11/GPX-4 trajectory. Naunyn Schmiedebergs Arch Pharmacol. 2025;398(3):3163-75.

54. Nah J, Yuan J, Jung YK. Autophagy in neurodegenerative diseases: from mechanism to therapeutic approach. Mol Cells. 2015;38(5):381-9.

55. Deneubourg C, Ramm M, Smith LJ, Baron O, Singh K, Byrne SC, et al. The spectrum of neurodevelopmental, neuromuscular and neurodegenerative disorders due to defective autophagy. Autophagy. 2022;18(3):496-517.
56. Aghaei M, Motallebnezhad M, Ghorghanlu S, Jabbari A, Enayati A, Rajaei M, et al. Targeting autophagy in cardiac ischemia/reperfusion injury: A novel therapeutic strategy. J Cell Physiol. 2019;234(10):16768-78.
57. Tang L, Zhang W, Liao Y, Wang W, Deng X, Wang C, et al. Autophagy: a double-edged sword in ischemia-reperfusion injury. Cell Mol Biol Lett. 2025;30(1):42.